Performance enhancement of MIMO-FSO communication systems using hybrid optical amplifiers

C. PALANIAPPAN*, S. ROBINSON
Department of Electronics and Communication Engineering, Mount Zion College of Engineering and Technology Pudukkottai, Tamil Nadu, India

Free-space optical (FSO) communication is a green wireless data transmission technique that utilises light beams as a modulated carrier and is known for its high capacity. Numerous advantages of FSO technology include compatibility with unlicensed frequency bands, reduced latency, inexpensive installation costs, and large bandwidth. Because of this, it can be used for both the first and last terminal connections. However, weather-induced attenuation, especially from rain, fog, and haze, can weaken the signal-to-noise ratio (SNR) and restrict the performance of FSO systems. This work proposes a MIMO-FSO (Multiple-Input Multiple-Output FSO) system coupled with double- and triple-boost optical amplifiers to improve transmission quality and signal power, thereby addressing these issues. The system's performance is evaluated at three standard wavelengths — 850 nm, 1310 nm, and 1550 nm—using non-return-to-zero (NRZ) modulation. Experimental results show that a 32×32 MIMO configuration with a triple-stage amplifier at 1550 nm achieves a maximum transmission distance of 114.8 km under clear weather conditions. The system maintains operable ranges of 14.84 km in rain, 10.48 km in fog, and 8.32 km in haze in unfavourable environments. The system's dependability across various atmospheric conditions is confirmed by thorough evaluations of the Q-factor, bit-error rate (BER), and eye diagrams.

(Received October 4, 2025; accepted April 8, 2026)

Keywords: FSO, MIMO, NRZ, Boost Amplifiers, BER, Q factor

1. Introduction

Optical Wireless Communication (OWC) systems have emerged as a transformative solution to the limitations of conventional RF and fibre-optic networks, offering ultra-high data rates, broader bandwidths, enhanced data security, and cost-effective deployment [1]. Among these, FSO technology distinguishes itself by transmitting modulated light signals through free space, thereby obviating the need for physical cabling while leveraging principles similar to those of Optical Fibre Communication [2]. FSO is particularly advantageous in scenarios where fibre installation is either impractical or economically burdensome, such as last-mile access, inter-building links, cellular backhaul, and ground-satellite communication [3, 4]. FSO systems align well with the requirements of 5G and emerging 6G networks, primarily due to their license-exempt spectrum, compact transceiver design, and immunity to electromagnetic interference [5, 6]. However, atmospheric phenomena, including fog, rain, and turbulence, can significantly deteriorate FSO performance through absorption, scattering, and scintillation. Fog is the most detrimental, with attenuation potentially exceeding 100 dB/km. Additionally, the need for strict line-of-sight alignment renders FSO links vulnerable to structural vibrations and dynamic misalignments [7]. To mitigate these impairments, various enhancement strategies have been explored, including adaptive optics, forward error correction (FEC), hybrid RF/FSO configurations, and spatial diversity techniques such as MIMO.

Among them, MIMO-FSO has gained significant traction due to its ability to counteract turbulence-induced fading and improve overall link reliability. When modelled under realistic atmospheric conditions using Gamma–Gamma and Log-Normal distributions, MIMO systems have demonstrated considerable gains in the BER, SNR, and stability [8–11]. In [12], the author introduced a simplified BER model based on an infinite series for Gamma–Gamma turbulence, offering reduced computational complexity for both SISO and MIMO systems. The author's comparative evaluation in [13] of 4×4 MIMO FSO systems across the 850–1550 nm wavelength range confirmed that higher wavelengths and spatial diversity extended link distances to up to 94 km in clear weather. Under heavy fog (~26 dB/km), MIMO modestly improved performance, extending the reach from 1.4 km to 1.58 km [14]. In more severe conditions (~59 dB/km), a 9×9 MIMO system employing NRZ and Mach–Zehnder modulation achieved BERs as low as 10^{-9} and Q-factors of approximately 6, demonstrating robustness [15]. The modulation format also plays a critical role. NRZ modulation exhibits better resilience under high attenuation, whereas RZ modulation is more effective in low-loss scenarios [16]. Advanced OOK-based variants, such as CSNRZ, DBNRZ, and MDBNRZ, have further improved the received optical power by 21–25%, increasing the tolerance to alignment errors and channel loss [17]. The author proposed a multi-hop MISO FSO relay system using M-ary PPM with spatial modulation to combat atmospheric turbulence and misalignment over Gamma–Gamma channels. Operating at 1550 nm, the

system achieves 2.5 Gb/s over 11 km at BER = 10^{-9}, while MISO-assisted PPM/DPPM significantly outperforms conventional OOK-based FSO systems in terms of BER, SNR, and power efficiency [18].

Recent research has shifted from relying on idealised assumptions and neglecting amplifier effects to focusing on practical solutions that incorporate Hybrid Optical Amplifiers (HOAs). These amplifiers, which integrate EDFAs, SOAs, and Raman amplifiers, are employed to enhance Wavelength Division Multiplexing (WDM)-FSO systems, particularly in terms of range and signal quality under adverse weather conditions. Their significance is increasingly recognised in the context of scalable 5G/6G deployments [19-23]. In [24], the author proposed a hybrid WDM–FSO access network at 1550 nm to analyse atmospheric turbulence and interchannel crosstalk effects. In Gamma–Gamma turbulence, DPPM outperforms OOK with lower BER and higher power efficiency, particularly on upstream links, demonstrating its suitability for high-capacity, turbulence-resilient optical access networks. Studies utilising Continuous Phase Frequency Shift Keying (CPFSK) with optimised beam parameters have demonstrated substantial improvements in BER and Q-factor under clear-sky conditions [25].

The author proposed a WDM–FSO access network at 1550 nm to study the impact of atmospheric turbulence and interchannel crosstalk. Comparing OOK and DPPM under Gamma–Gamma turbulence, results show that DPPM offers superior power efficiency and improved BER, especially in upstream transmission. In contrast, turbulence and ASE noise dominate link degradation [26]. Simulations involving 3–15 Tx/Rx pairs across diverse weather conditions have confirmed performance enhancements in tropical regions [27]. In [28], the author proposed a MIMO–DWDM FSO system at 1550 nm delivering 20 Gb/s (8 × 2.5 Gb/s) over 1500 m under Gamma–Gamma turbulence. Results show that QO-STBC and STTC with MRC achieve the lowest BER and outage probability, offering notable SNR gains and a reduced power penalty (~23 dB at BER = 10^{-9}) for high-capacity, turbulence-resilient FSO links.

Field trials conducted in Puducherry on a 16×16 MIMO-FSO link at 1550 nm and 10 Gbps have demonstrated robust performance in moderate weather conditions. However, dense fog (>70 dB/km) remains a limitation [29]. Most recently, a 32×32 MIMO-FSO configuration incorporating dual-stage amplification, Bessel filtering, and Maximal Ratio Combining (MRC) has achieved Q-factors exceeding 70 in rain and above 58 in fog with negligible BER, underscoring the practicality of large-scale MIMO architectures in real-world atmospheric conditions [30-31].

Despite continued advancements, MIMO-FSO systems still face notable limitations. The influence of wavelength-dependent behaviour under severe weather conditions has not been comprehensively studied, particularly in systems integrating MIMO with advanced optical amplification. Additionally, the lack of robust simulation frameworks that support scalable architectures and realistic turbulence models limits the comprehensive performance evaluation of such systems.

Main contribution of the work

This study presents a comprehensive simulation of FSO systems by integrating advanced MIMO configurations, NRZ modulation, and the Gamma–Gamma turbulence model for realistic atmospheric modelling, as outlined below. These elements collectively aim to enhance data capacity, improve link reliability, and increase transmission range in challenging environments.

- Scalable MIMO Architecture: MIMO configurations ranging from 2×2 to 32×32 are employed to enhance spatial diversity, increase throughput, and improve link robustness under varying weather conditions.
- Enhanced Amplification Design: Double- and triple-boosted amplifier setups are implemented at the transmitter, receiver, and mid-link positions to maintain signal strength and extend communication range.
- Gamma–Gamma Turbulence Modelling: Atmospheric turbulence effects, including beam fading and scintillation, are modelled using the Gamma–Gamma distribution, offering accurate performance prediction under moderate to strong turbulence.
- Multi-Wavelength Analysis: System performance is evaluated at 850 nm, 1310 nm, and 1550 nm, providing comparative insights into wavelength-dependent behaviour.

A unified simulation framework is developed for flexible, parameter-driven analysis under diverse environmental conditions. This approach supports scalable, high-capacity optical wireless links ideal for 5G/6G backhaul and last-mile access in weather-impacted regions.

The paper is structured as follows: Section 2 details the system model and simulation methodology; Section 3 presents and analyses the results; Section 4 provides a comparative performance analysis; and Section 5 concludes the study.

2. Simulation design and performance analysis of the proposed SISO and MIMO FSO systems

2.1. FSO system

Fig. 1 shows the fundamental setup of a Free Space Optical (FSO) communication system. An electrical input is modulated and converted into an optical signal by a light source using an E/O converter. The optical signal is transmitted through free space using collimating lenses. The signal is received at the receiving end with a photodetector, which converts it to an electrical signal using an O/E converter, and then demodulates it to retrieve the original data.

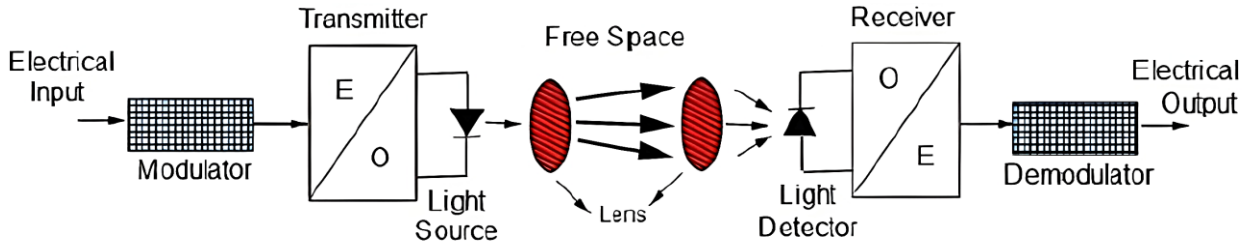

Fig. 1. Block diagram of an optical wireless link (colour online)

2.2. Atmospheric attenuation models

Link budget:

The link budget of an FSO communication system is significantly affected by attenuation. Several factors, including the operating wavelength, transmission distance, detector type, optical modulator characteristics, and the efficiency of both the transmitting and receiving units, substantially influence the overall system performance. Collectively, these variables determine the signal quality and propagation losses within the optical channel. The Friis transmission equation, which relates the transmitted power to the received power while accounting for propagation losses and system-specific characteristics, is commonly used in link budget analysis to estimate the optical power received at the detector.

The Friis transmission format provides the pointing-loss factors presented in [32, 33].

$$P_R = P_T \eta_T \eta_R L_S G_T G_R L_T L_R \exp(-\alpha Z) \quad (1)$$

where P_T and P_R is the transmitted and received, η_T and η_R is the transmitter and receiver efficiency, G_T and G_R is the transmitter and receiver effective antenna gain, L_T and L_R is the transmitter and receiver pointing loss factor, L_S is the space loss factor and α is the coefficient of atmospheric attenuation depends on the type of scattering, signal wavelength, size of the particles of the atmosphere and the link visibility.

The space loss factor L_S, is given by

$$L_S = (\lambda/4\pi L)^2 \quad (2)$$

where λ is the signal wavelength, L is the link distance between the transmitter and receiver.

Due to the wavelength dependence, the optical system loss in free space is much larger than in the RF system, so the *Ls* loss factor is much smaller.

The transmitter and receiver gain, G_T and G_R, can be estimated by

$$G_T = (\pi D_T/\lambda)^2 \quad (3)$$

$$G_R = (\pi D_R/\lambda)^2 \quad (4)$$

where D_T and D_R are the transmitter and receiver aperture diameters.

The transmitter and receiver pointing-loss factors, L_T and L_R, can be estimated using [32].

$$L_T = \exp(-G_T (\theta_T)^2) \quad (5)$$

$$L_R = \exp(-G_R (\theta_R)^2) \quad (6)$$

where θ_T and θ_R is the transmitter and receiver pointing error angles.

In the FSO link, the power budget is given by [32]

$$P_{RX} = P_{TX} - \alpha_{sys} - \alpha_{atm} \quad (7)$$

where α_{sys} is system attenuation, and α_{atm} is total atmospheric attenuation.

Pointing error poses a significant challenge in FSO communication links, as it directly affects the received optical power and the system's overall reliability. This error typically results from factors such as adverse atmospheric conditions, misalignment between the transmitter and receiver, beam wander induced by turbulence, and structural movements, including building sway. Using Eqs. (5) and (6), the pointing error at both the transmitter and receiver is estimated to be 1.277 μrad. The transmission loss factors for the transmitter (L_T) and receiver (L_R) are each assumed to be 4 dB [32].

Fog attenuation (Kruse model):

The Kruse model is frequently utilised to estimate fog-induced attenuation across visible and infrared wavelengths, as it effectively correlates atmospheric visibility data with optical signal loss [31, 32]

$$\beta_a(\lambda) = \frac{13}{v}\left(\frac{\lambda}{0.55}\right)^{-q} \quad (8)$$

In this context, υ is the atmospheric visibility (km), q is a coefficient related to the particle size distribution in the atmosphere, and λ denotes the optical signal wavelength (nm).

$$q_f = \begin{cases} 1.6 & for\ v_f > 50\ km \\ 1.3 & for\ 6\ km < v_f < 50\ km \\ 0.585 v_f^{\frac{1}{3}} & for\ v_f < 6\ km \end{cases} \quad (9)$$

Enhanced fog model (Kim's modification)

Kim enhanced the fog attenuation prediction model by refining the q_f −coefficient parameters, thereby improving the model's precision in low-visibility conditions [31, 33].

$$q_f = \begin{cases} 1.6 & for\ v_f > 50\ km \\ 1.3 & for\ 6\ km < v_f < 50\ km \\ 0.16v_f + 0.34 & for\ 1\ km < v_f < 6\ km \\ v_f - 0.5 & for\ 0.5\ km < v_f < 1\ km \\ 0 & for\ v_f < 0.5\ km \end{cases} \quad (10)$$

When visibility is less than 500 meters, the model becomes independent of the operating wavelength.

Rain attenuation model

Rain causes scattering that is generally independent of wavelength. The empirical model is used [25]:

$$\beta_{rain} = 1.067R^{0.67} \quad (11)$$

where R denotes the rain rate, measured in millimetres per hour (mm/h).

The attenuation caused by snowfall as a function of visibility is expressed as follows.

$$\alpha_{rain} = \frac{2.8}{V_a} \quad (12)$$

Haze attenuation model

Haze attenuation is estimated using:

$$\beta_{haze} = \frac{3.91}{V}\left(\frac{\lambda}{550nm}\right)^{-q} \quad (13)$$

In this equation, β corresponds to haze-related attenuation, λ represents the optical signal wavelength (in nanometers), V denotes visibility (in kilometres), and q characterises the particle size distribution relevant to haze scattering.

2.3. SISO-FSO systems

FSO communication is highly influenced by atmospheric turbulence and propagation losses. This study uses the Gamma–Gamma model to characterise weak to moderate turbulence conditions. A simulation framework is developed to assess the performance of SISO-FSO systems, with a focus on improving BER and Q-factor via optical amplification.

Two amplification schemes are considered: a double-boosted setup with amplifiers at the transmitter and receiver, and a triple-boosted design with an additional in-line amplifier. These enhance signal integrity over long distances. The SISO FSO model serves as a baseline, comprising system components such as the transmitter, free-space channel, and receiver, as illustrated in Fig. 2.

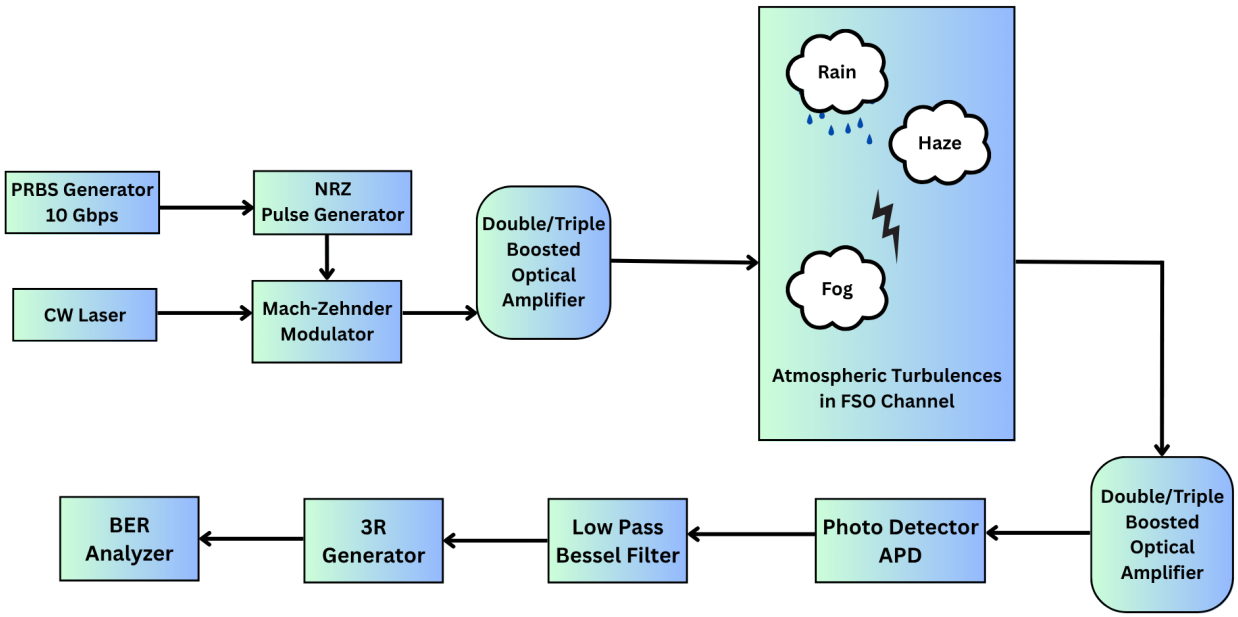

Fig. 2. Block diagram of SISO FSO system (colour online)

The transmitter section comprises a Pseudo-Random Binary Sequence (PRBS) generator operating at 10 Gbps, an NRZ pulse generator, a Mach–Zehnder modulator, and a laser diode emitting at 850 nm, 1310 nm, or 1550 nm. The modulated optical signal is amplified by a double- or triple-stage optical amplifier before being transmitted through the FSO channel.

The FSO channel is modelled to account for atmospheric turbulence using the Gamma–Gamma distribution and visibility-dependent attenuation to

simulate realistic weather conditions. At the receiver end, an Avalanche Photodiode (APD) detects the signal, followed by additional optical amplification (double or triple stage), a Low-Pass Bessel filter, and a 3R regenerator for signal reshaping, retiming, and re-amplification.

Atmospheric attenuation plays a critical role in signal quality. Table 1 lists the attenuation values applied in the simulations for the different weather scenarios considered in this attempt [17].

Table 1. Weather conditions used in the simulation

Weather Condition	Attenuation (dB/km)
Clear air	0.44
Rain	4.6
Fog	6.8
Haze	8.8

All simulation parameters [17] are summarised in Table 2.

To facilitate this investigation, simulation models were developed. The SISO-FSO system layout is illustrated in Fig. 3, which shows the basic configuration comprising an optical transmitter, FSO channel, amplifier blocks, and receiver setup.

Table 2. Simulation parameters

Parameters	Values
Bit rate	10 Gbps
Wavelength	850 nm/1310 nm/ 1550 nm
Laser Power	10 dBm
Transmitter beam aperture	5 cm
Receiver beam aperture	20 cm
Beam Divergence	2 mrad
Additional losses	1 dB
APD Gain	3 dB
Photodetection responsivity	1 A/W
Photodetector dark current	10 nA
Model	Gamma-Gamma Model
Optical amplifier	Gain 20 dB
	Noise figure 10 dB
Pointing Error	1.277 μrad

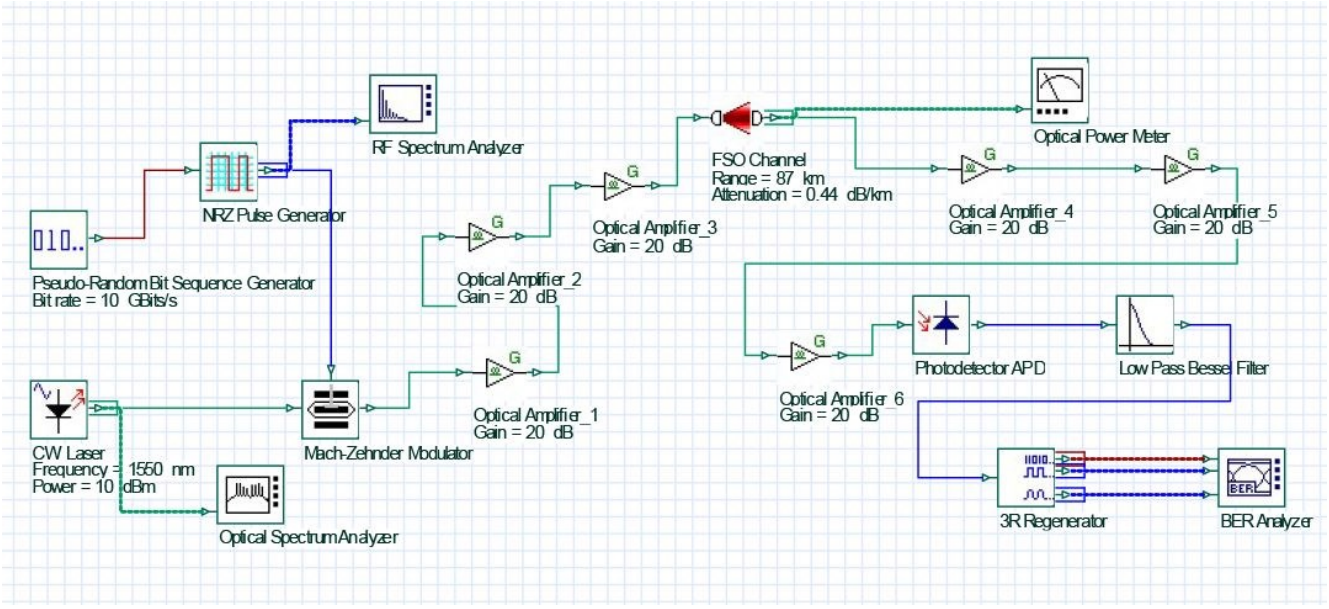

Fig. 3. The proposed simulation layout of the SISO-FSO system (colour online)

2.4. MIMO-FSO Systems

A CW laser serves as the optical source in the MIMO-FSO architecture, followed by key components such as the M-Z modulator, NRZ pulse generator, and optical amplifiers. The baseband electrical signal is converted to an optical signal by the modulator, enabling transmission through the atmosphere. A photodetector, a low-pass Bessel filter, optical amplifiers, and a BER analyser make up the receiver. This modular design enables simulation of the complete optical communication chain. The system model for the MIMO-FSO architecture is presented in Fig. 4.

To support this investigation, specialised simulation models were developed. A 32×32 MIMO-FSO system was constructed, as shown in Fig. 5. This architecture incorporates spatial diversity and distinct optical amplifier configurations, with each transmission and reception path simulated independently. Such a setup enables the precise modelling of MIMO signal propagation and combining behaviour under realistic operational conditions.

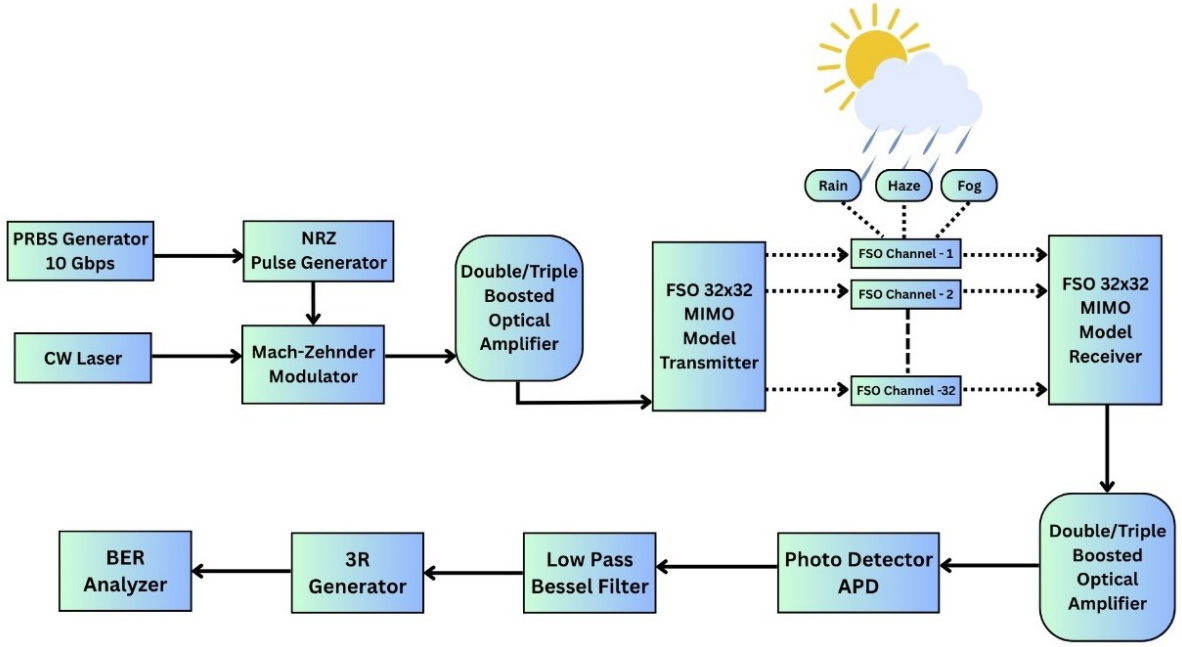

Fig. 4. Block diagram of MIMO-FSO system (colour online)

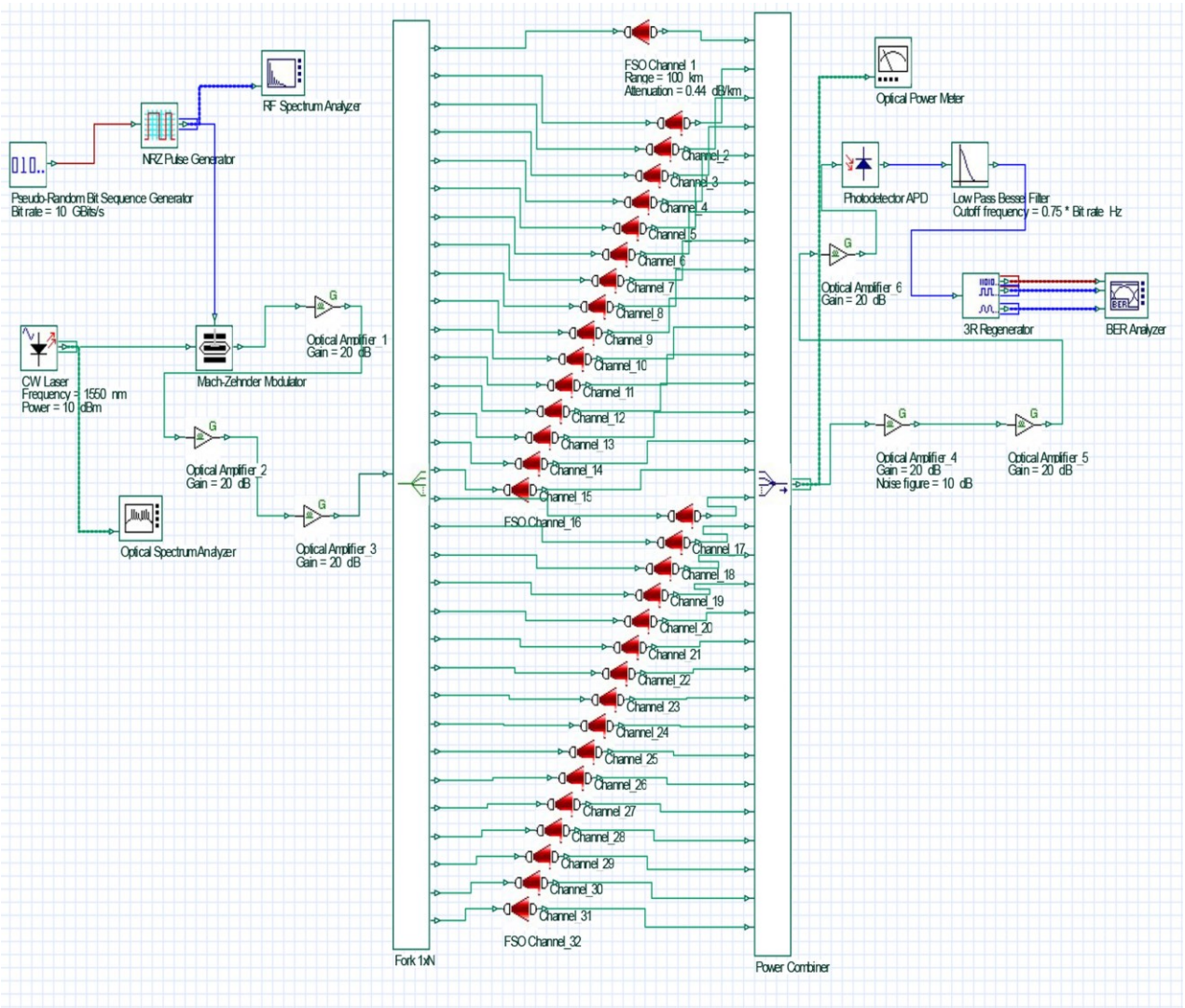

Fig. 5. The proposed simulation layout of a 32 × 32 MIMO-FSO system (colour online)

3. Performance analysis of SISO and MIMO FSO system

This section presents a comprehensive performance analysis of FSO communication systems under various atmospheric conditions, namely clear weather, rain, fog, and haze. The analysis considers both SISO and MIMO architectures (2×2, 4×4, 8×8, 16×16, and 32×32), with two distinct amplification schemes: Double Boost and Triple Boost. System performance is assessed in terms of link range, BER, Q-factor and received power across three operating wavelengths, 850 nm, 1310 nm, and 1550 nm.

3.1. Performance under clear weather conditions

Fig. 6 optical spectra of the transmitted 10 Gbps signal at 850 nm, 1310 nm, and 1550 nm. The presence of narrow carrier peaks demonstrates high wavelength stability and low laser linewidth. Symmetric modulation sidebands further indicate efficient bandwidth utilisation in the proposed FSO/MIMO-FSO system.

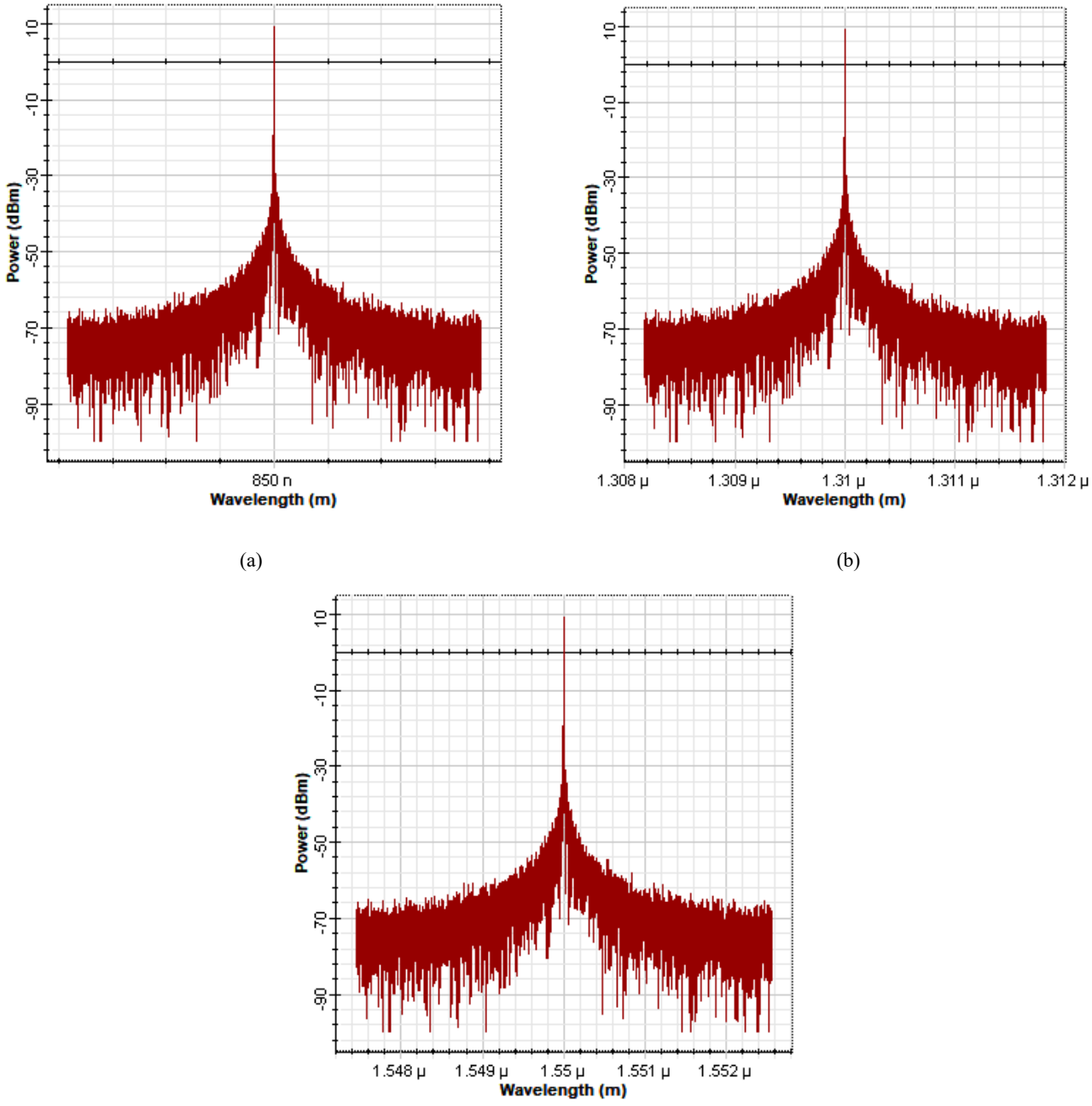

Fig. 6. Optical spectra of the MIMO-FSO communication system: (a) optical spectrum at 850 nm, (b) optical spectrum at 1310 nm, (c) optical spectrum at 1550 nm (colour online)

Under all atmospheric conditions, the increase in BER with greater link distance is primarily attributed to the gradual reduction in received optical power, as discussed in Section III-A. Higher-order MIMO configurations improve robustness by introducing spatial diversity, while multi-stage amplification extends the available link margin. Therefore, the subsequent results examine achievable transmission ranges across different channel severities.

Fig. 7(a) depicts the BER performance of SISO and multiple MIMO-FSO configurations as a function of link distance under clear atmospheric conditions using a double boost amplifier. The SISO system maintains a target BER of 10^{-9} only up to approximately 51 km, beyond which error performance deteriorates rapidly due to atmospheric attenuation, beam divergence, and turbulence-induced intensity fading.

Incorporating MIMO spatial diversity significantly enhances link robustness by mitigating deep fades and improving signal stability at the receiver. Consequently, the achievable transmission range increases to approximately 57 km for 2×2 MIMO, 62.8 km for 4×4 MIMO, 67.6 km for 8×8 MIMO, and 73.4 km for 16×16 MIMO. The 32×32 MIMO configuration demonstrates the highest resilience, sustaining a BER of 10^{-9} over 77.2 km, an improvement of roughly 26 km over SISO. These gains are primarily attributed to diversity gain, enhanced received optical power, and reduced turbulence-induced irradiance fluctuations, which collectively improve the system performance.

Fig. 7(b) presents the BER performance with a triple-boost amplifier, revealing a substantial extension in the achievable link distance. The SISO system supports reliable transmission up to approximately 86 km at a BER of 10^{-9}, benefiting from the increased optical power. The integration of MIMO further extends system reach, with operational distances of 93 km for 2×2 MIMO, 99 km for 4×4 MIMO, 104.4 km for 8×8 MIMO, and 110.6 km for 16×16 MIMO. The 32×32 MIMO architecture achieves the longest link range of 114.8 km, yielding a 28 km improvement relative to SISO.

The superior performance of higher-order MIMO arises from the exploitation of spatial diversity, improved power combining across multiple apertures, and enhanced resistance to turbulence-induced fading, which collectively suppress BER growth at extended distances.

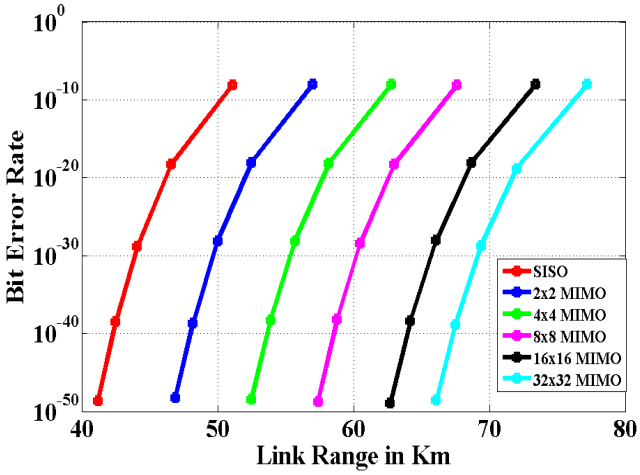

(a)

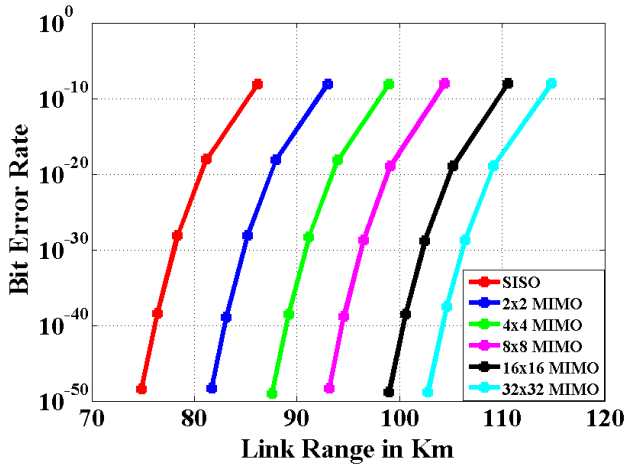

(b)

Fig. 7. BER versus link range for SISO and MIMO FSO communication systems under clear atmospheric conditions using (a) double boost amplifier and (b) triple boost amplifier configurations (colour online)

Fig. 8 shows the relationship between Q-factor and optical received power for SISO and several MIMO-FSO configurations under clear atmospheric conditions. The results use (a) double-stage and (b) triple-stage optical amplification. In all cases, the Q-factor increases with received power, reflecting performance limited by the SNR and determined by the detection margin, the minimum threshold needed to distinguish the signal from noise. Higher-order MIMO systems achieve superior Q-factors at lower received power because spatial diversity—provided by multiple transmitter-receiver pairs—reduces fading and improves reliability. The triple-stage amplifier shifts the curves to lower power levels, demonstrating greater tolerance to connection loss and noise. The 32×32 MIMO-FSO configuration performs best, highlighting the benefits of broad spatial diversity and stronger optical gain for maintaining signal integrity under clear-channel conditions.

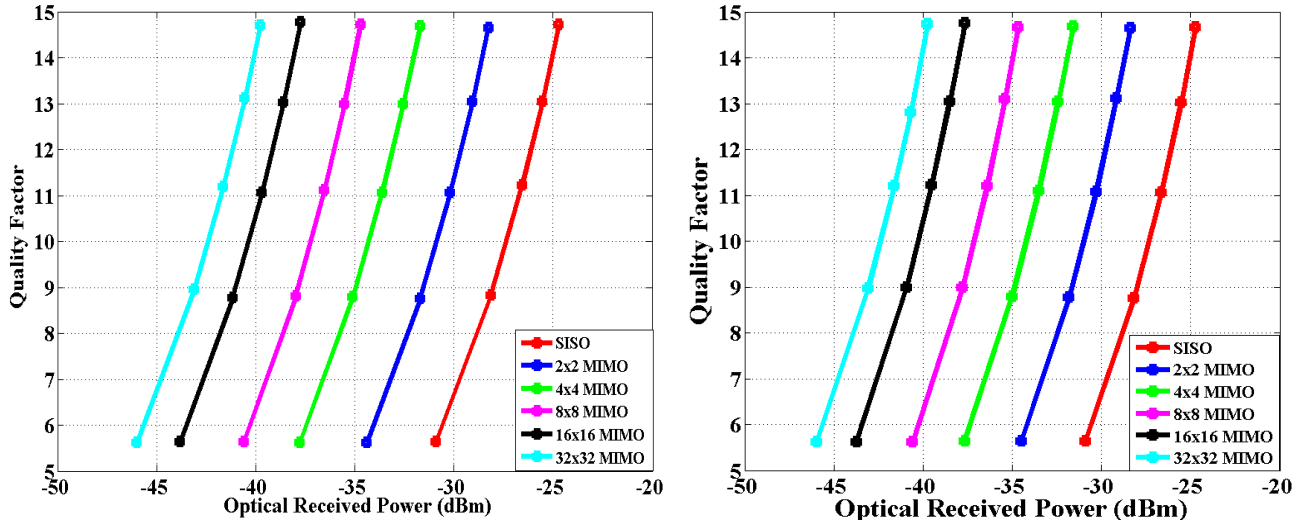

(a) (b)

Fig. 8. Q-factor versus received optical power for various MIMO FSO configurations under clear atmospheric conditions using (a) double boost amplifier and (b) triple boost amplifier (colour online)

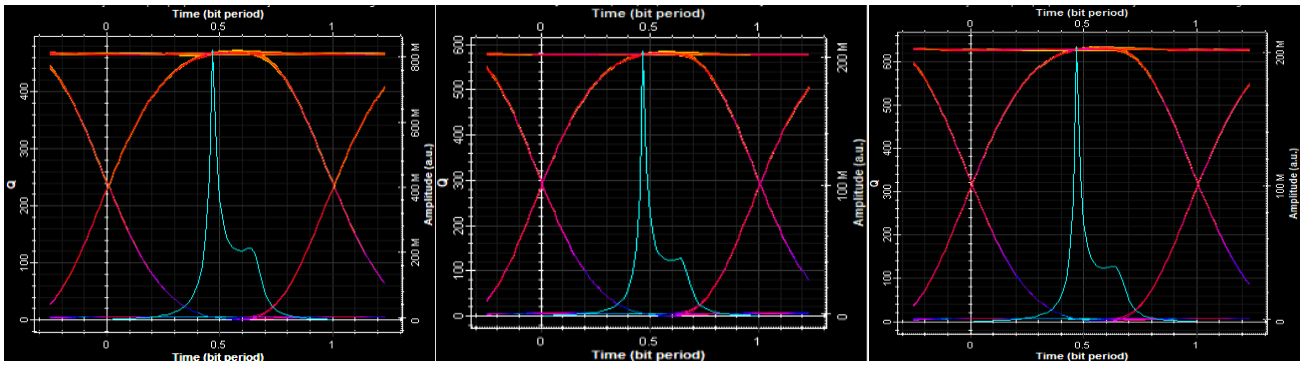

(a) 850 nm at 1 Km (b) 1310 nm at 1 Km (c) 1550 nm at 1 Km

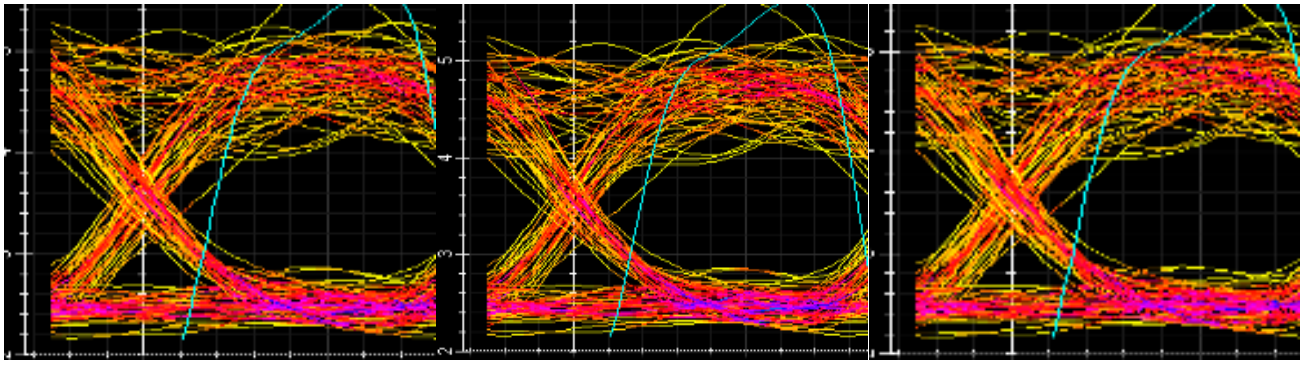

(d) 850 nm at 81.40 Km (e) 1310 nm at 84.90 Km (f) 1550 nm at 86.20 Km

Fig. 9. (a) Eye pattern performance of the SISO-FSO system using a triple boost amplifier at 850 nm, 1310 nm, and 1550 nm under clear atmospheric conditions (colour online)

Figs. 9(a) and 9(b) display eye-diagram results obtained under clear atmospheric conditions, with a specific attenuation of 0.44 dB/km. The SISO-FSO system enables reliable transmission over distances of approximately 81.40 km, 84.90 km, and 86.20 km at wavelengths of 850 nm, 1310 nm, and 1550 nm, respectively. In comparison, the 32×32 MIMO-FSO configuration, utilising triple-stage amplification, extends the achievable transmission range to approximately 109.80 km, 113.40 km, and 114.80 km at the same wavelengths.

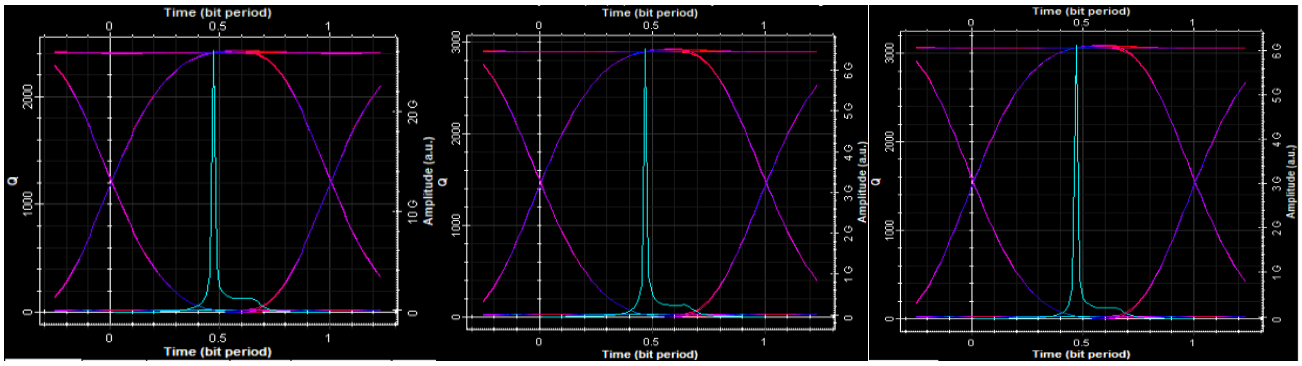

(a) 850 nm at 1 Km (b) 1310 nm at 1 Km (c) 1550 nm at 1 Km

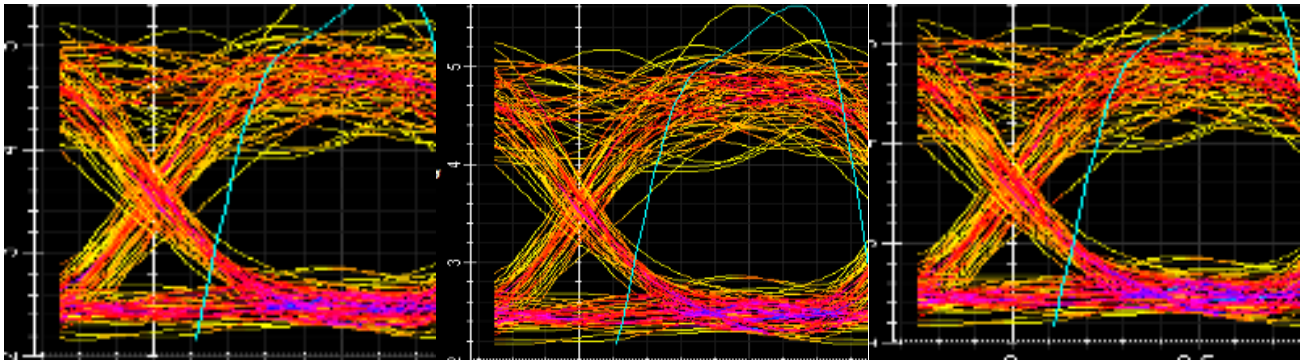

(d) 850 nm at 109.8 Km (e) 1310 nm at 113.40 Km (f) 1550 nm at 114.80 Km

Fig. 9. (b). Eye pattern performance of the 32 × 32 MIMO-FSO system using a triple boost amplifier at 850 nm, 1310 nm, and 1550 nm under clear atmospheric conditions (colour online)

3.2. Performance under rain conditions

Fig. 10 presents the BER performance under rainy conditions, indicating a significant reduction in achievable link range compared to clear weather. With double-stage amplification, reliable SISO transmission is limited to 8.30 km, while the 32×32 MIMO-FSO system extends the range to 11.55 km. Triple-stage amplification further improves the link margin, enabling SISO transmission up to 11.96 km and increasing the 32×32 MIMO-FSO range to approximately 14.84 km. This decrease in transmission distance, relative to clear conditions, is consistent with the anticipated degradation mechanism.

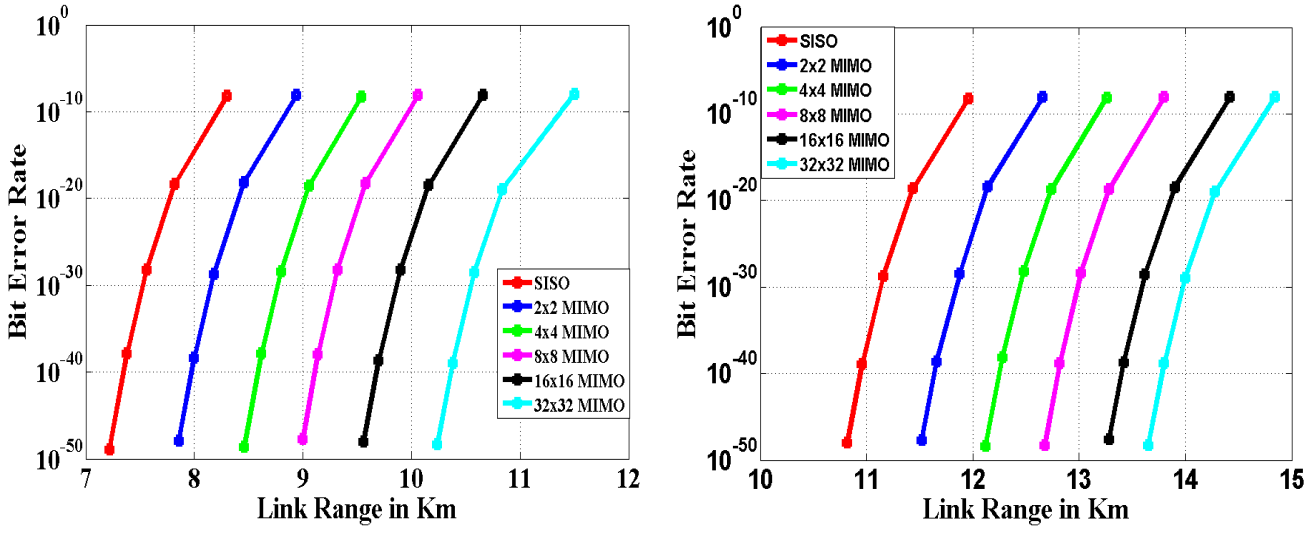

(a) (b)

Fig. 10. BER vs. distance for SISO and MIMO FSO links under rainy weather conditions using (a) double boost amplifier and (b) triple boost amplifier (colour online)

Fig. 11 presents Q-factor performance under rainy conditions. Compared with clear weather, achieving the same detection margin requires higher received power. However, the 32×32 MIMO-FSO configuration demonstrates superior Q-factor performance, and triple-stage amplification results in a measurable improvement in receiver sensitivity.

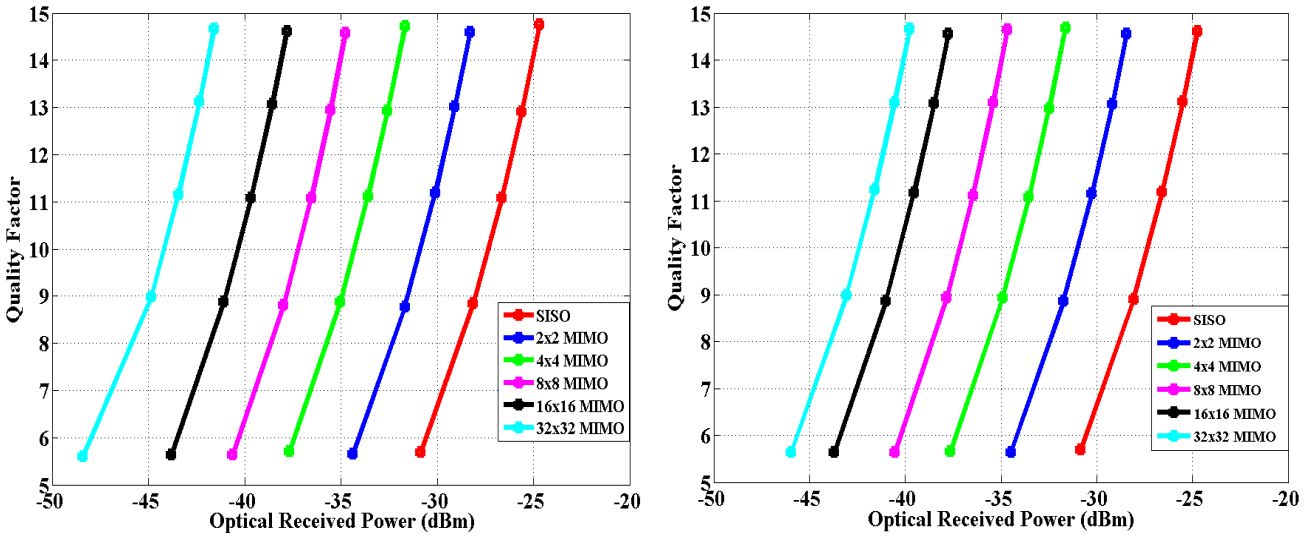

Fig. 11. Q-factor vs. optical received power for various MIMO-FSO configurations under rainy weather conditions using (a) double boost amplifier and (b) triple boost amplifier (colour online)

Figs. 12(a) and 12(b) present system performance under rainy conditions, characterised by a specific attenuation of 4.6 dB/km. Under these conditions, the SISO-FSO system maintains reliable transmission at distances of 11.48 km, 11.84 km, and 11.96 km for the three operating wavelengths. In comparison, the 32×32 MIMO-FSO system achieves transmission distances of approximately 14.34 km, 14.70 km, and 14.84 km with triple-stage amplification.

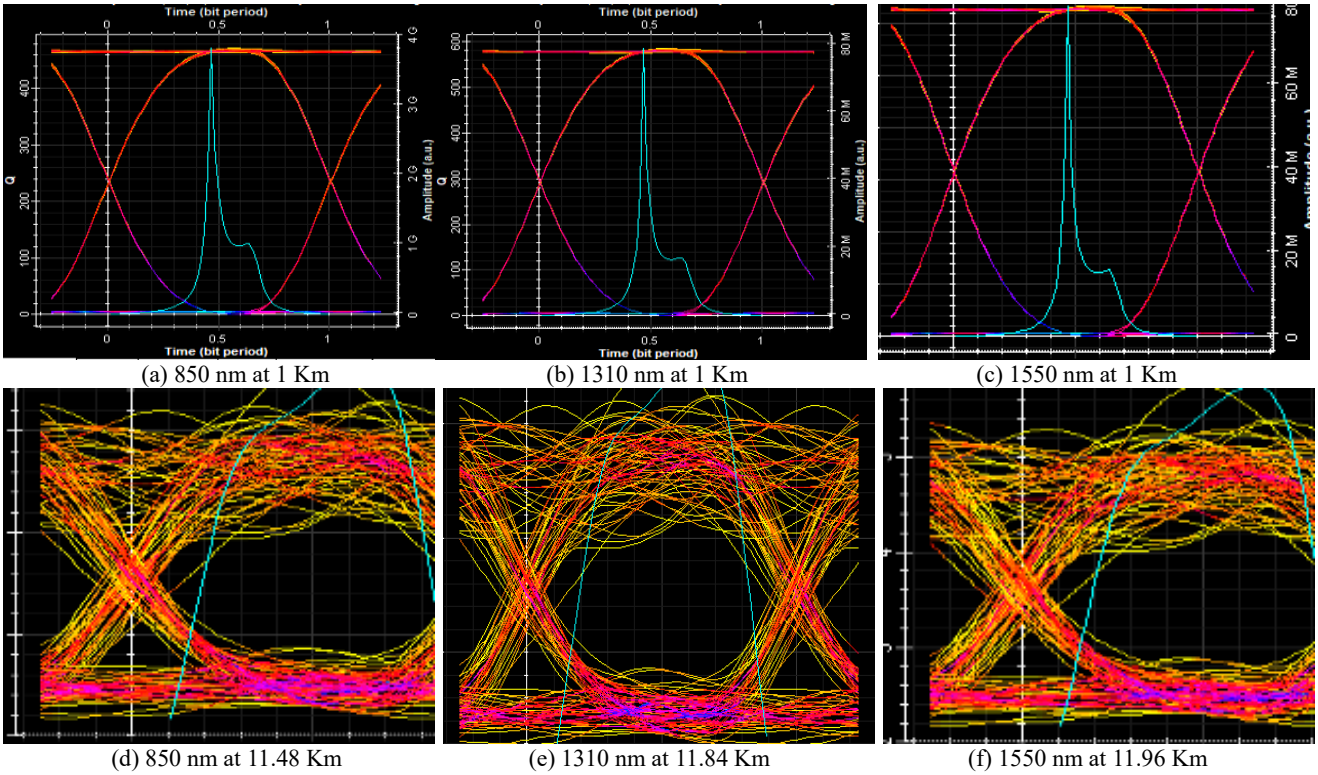

Fig. 12. (a) Eye pattern performance of the SISO-FSO system using a triple boost amplifier at 850 nm, 1310 nm, and 1550 nm under rainy weather conditions (colour online)

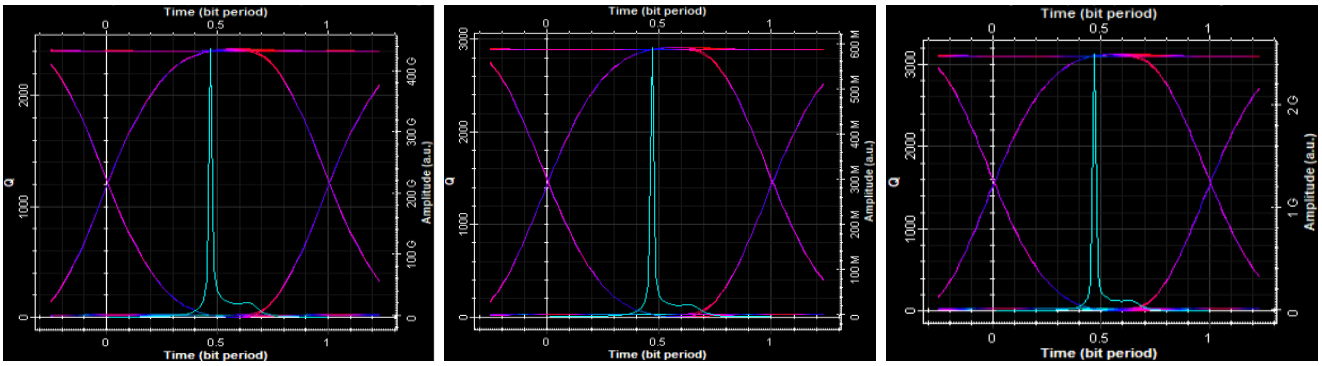

(a) 850 nm at 1 Km (b) 1310 nm at 1 Km (c) 1550 nm at 1 Km

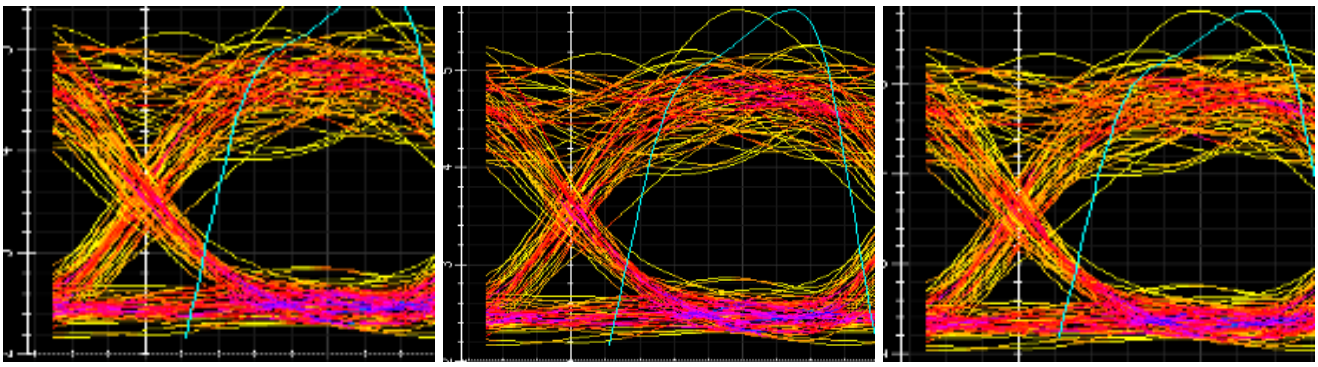

(d) 850 nm at 14.34 Km (e) 1310 nm at 14.70 Km (f) 1550 nm at 14.84 Km

Fig. 12. (b). Eye pattern performance of the 32 × 32 MIMO-FSO system using a triple boost amplifier at 850 nm, 1310 nm, and 1550 nm under rainy weather conditions (colour online)

3.3. Performance under fog conditions

Fig. 13 illustrates the BER variation under foggy conditions, which cause greater channel impairment than rain. With double-stage amplification, the SISO-FSO system supports transmission distances up to 6.02 km, while the 32×32 MIMO configuration extends the range to 8.17 km. Employing triple-stage amplification enables the SISO-FSO system to achieve a range of 8.52 km, and the 32×32 MIMO-FSO system to reach a maximum distance of 10.48 km.

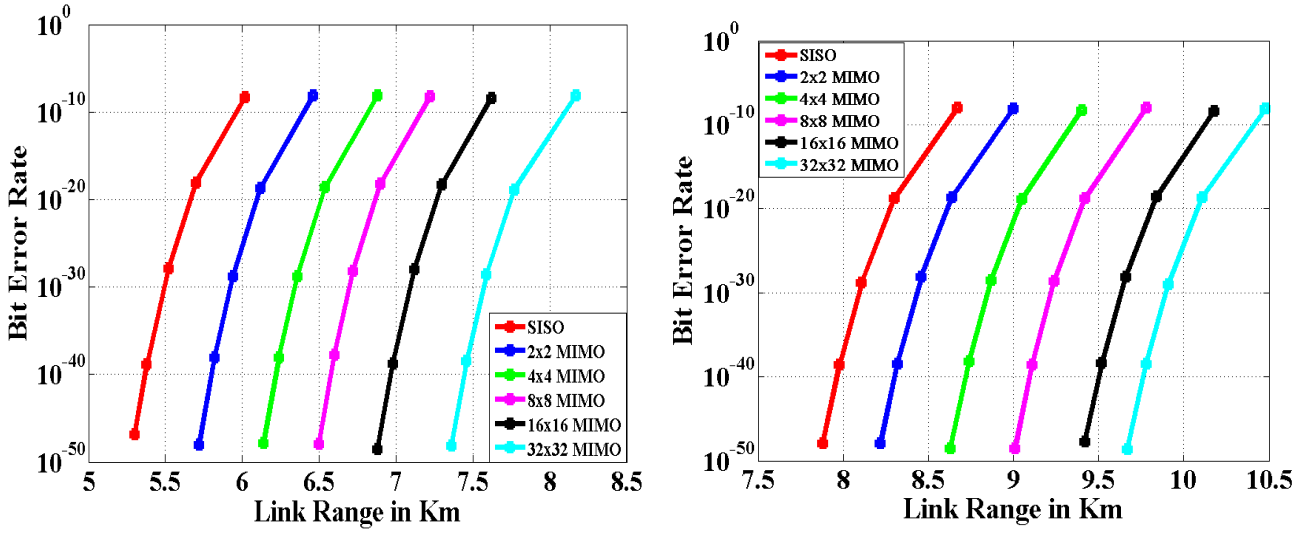

(a) (b)

Fig. 13. BER vs. Distance for SISO/MIMO FSO links under fog conditions with (a) double boost and (b) triple boost amplifiers (colour online)

Fig. 14 shows Q-factor variation under fog conditions, with a further shift toward higher received power. Despite the severe channel impairment, higher-order MIMO configurations retain improved detection margins, and triple-stage amplification continues to extend the operating range.

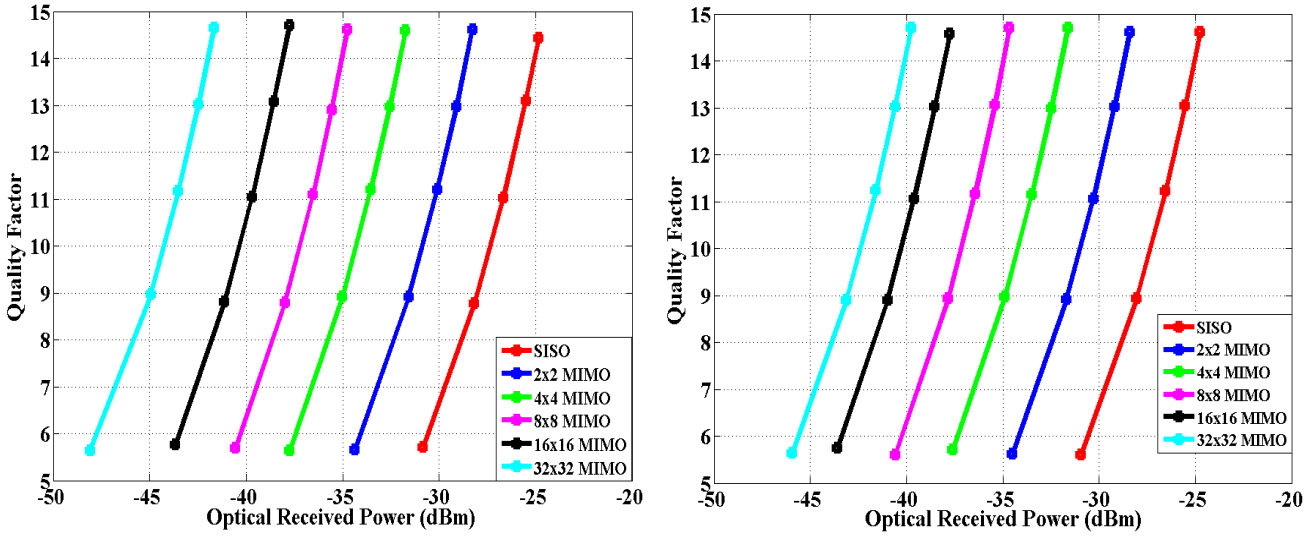

(a) (b)

Fig. 14. Q-factor vs. optical received power for various MIMO configurations under fog conditions using (a) double boost amplifier and (b) triple boost amplifier (colour online)

Figs. 15(a) and 15(b) present system performance under fog conditions with a specific attenuation of 6.8 dB/km. Reliable SISO-FSO transmission is maintained up to approximately 8.20 km, 8.44 km, and 8.52 km. In contrast, the 32×32 MIMO-FSO configuration extends the link range to 10.14 km, 10.39 km, and 10.48 km when triple-stage amplification is applied.

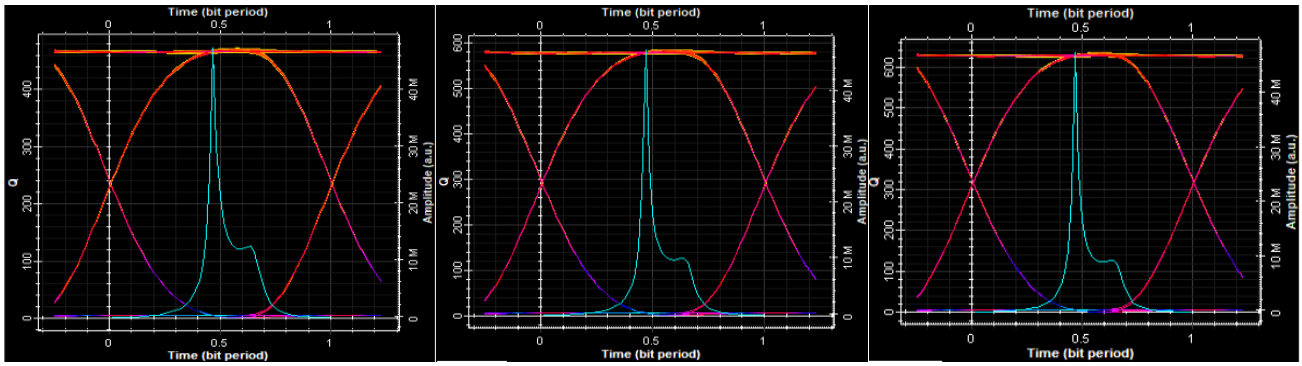

(a) 850 nm at 1 Km (b) 1310 nm at 1 Km (c) 1550 nm at 1 Km

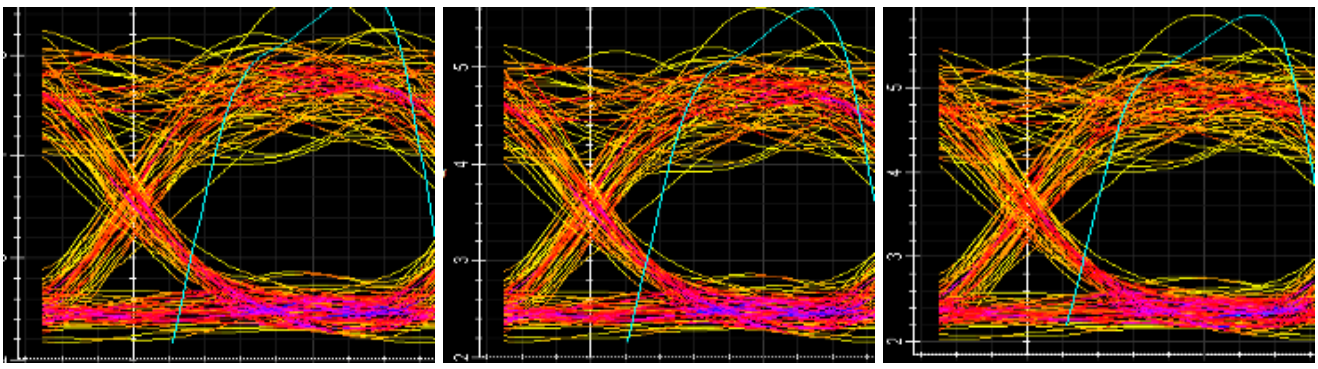

(d) 850 nm at 8.20 Km (e) 1310 nm at 8.44 Km (f) 1550 nm at 8.52 Km

Fig. 15. (a). Eye pattern performance of the SISO-FSO system using a triple boost amplifier at 850 nm, 1310 nm, and 1550 nm under fog conditions (colour online)

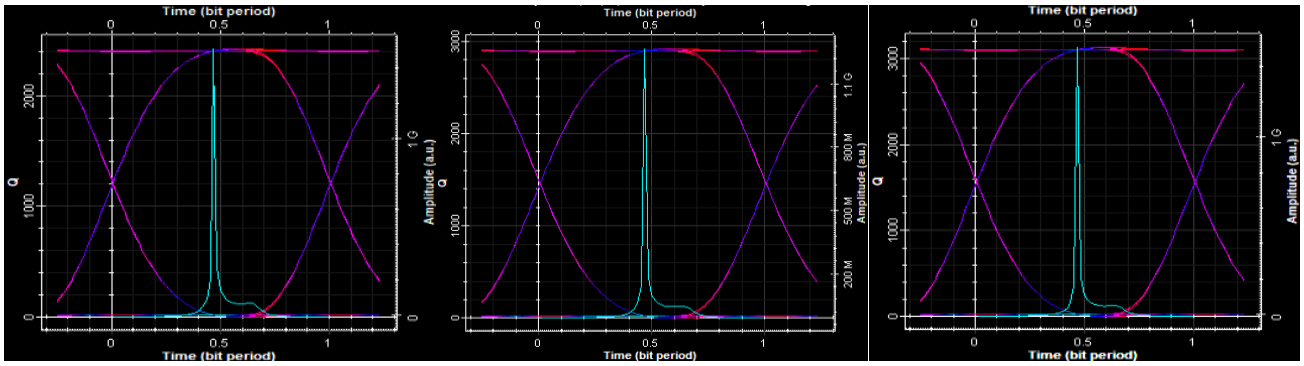

(a) 850 nm at 1 Km (b) 1310 nm at 1 Km (c) 1550 nm at 1 Km

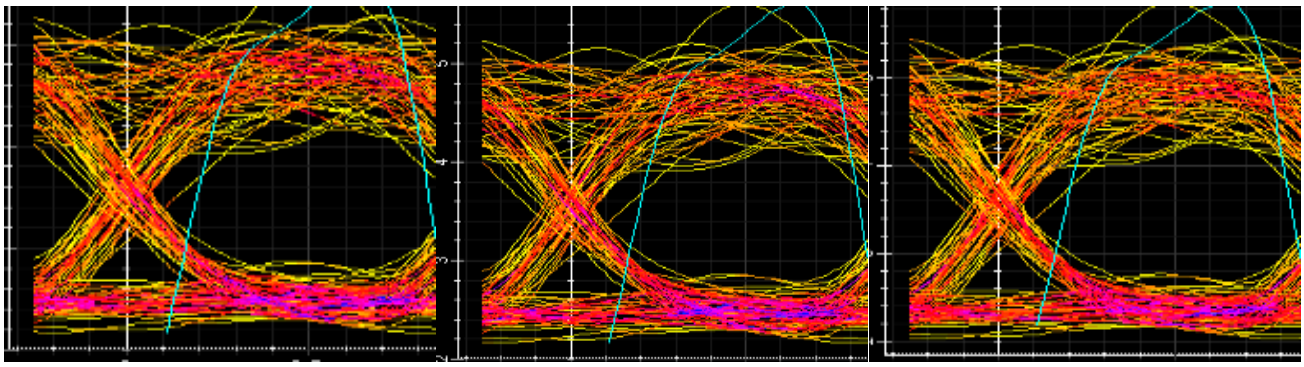

(d) 850 nm at 10.14 Km (e) 1310 nm at 10.39 Km (f) 1550 nm at 10.48 Km

Fig. 15. (b). Eye pattern performance of the 32 × 32 MIMO-FSO system using a triple boost amplifier at 850 nm, 1310 nm, and 1550 nm under fog conditions (colour online)

3.4. Performance under haze conditions

Fig. 16 presents the BER performance under haze conditions, identified as the most restrictive scenario in this study. With double-stage amplification, the SISO system achieves a BER of 10^{-9} up to 4.86 km, whereas the 32×32 MIMO-FSO system extends this range to 6.32 km. Triple-stage amplification further increases the SISO range to 6.80 km and extends the 32×32 MIMO-FSO link to approximately 8.32 km. The pronounced range limitation under haze conditions is consistent with the previously described dominant channel-loss mechanisms.

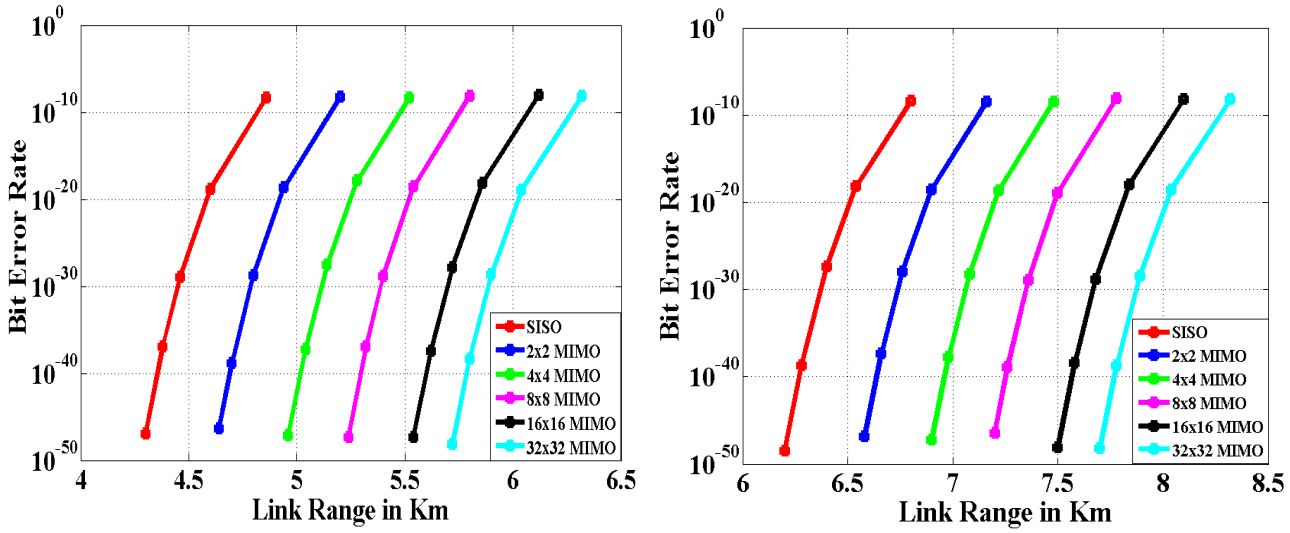

(a) (b)

Fig. 16. BER vs. distance for SISO/MIMO FSO links under haze conditions using (a) double boost and (b) triple boost amplifiers (colour online)

Fig. 17 presents Q-factor performance under haze conditions, which impose the most stringent power requirements among the scenarios considered. Despite significant aerosol attenuation, the 32×32 MIMO-FSO system demonstrates the highest Q-factor. Additionally, triple-stage amplification reduces the power threshold necessary for reliable detection.

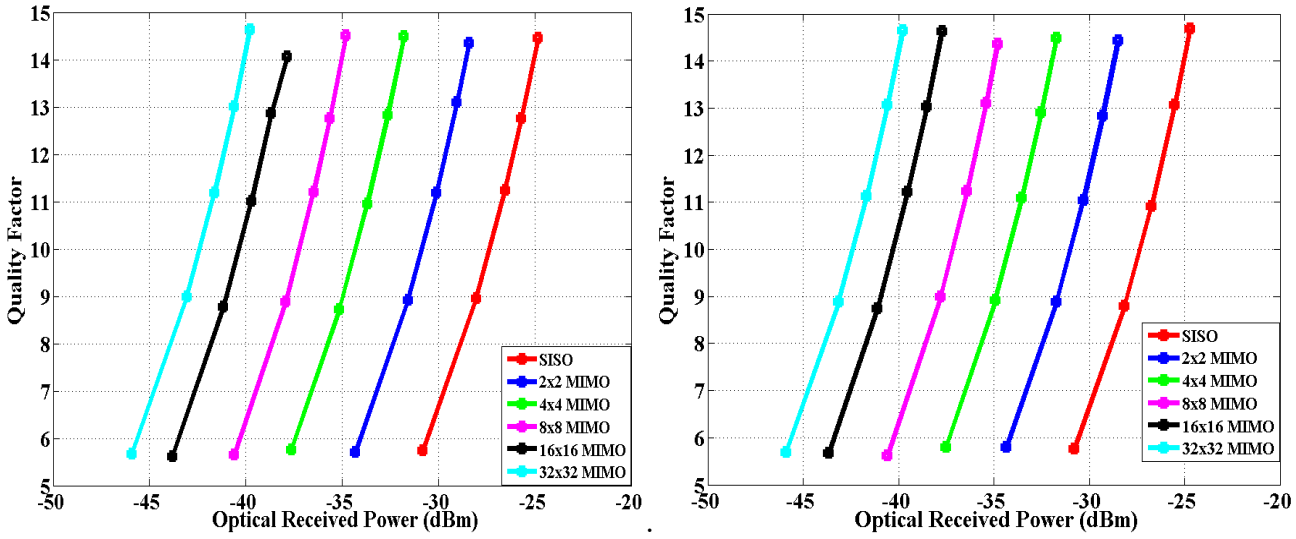

Fig. 17. Q-factor vs. optical received power for various MIMO configurations under haze conditions using (a) double boost amplifier and (b) triple boost amplifier (colour online)

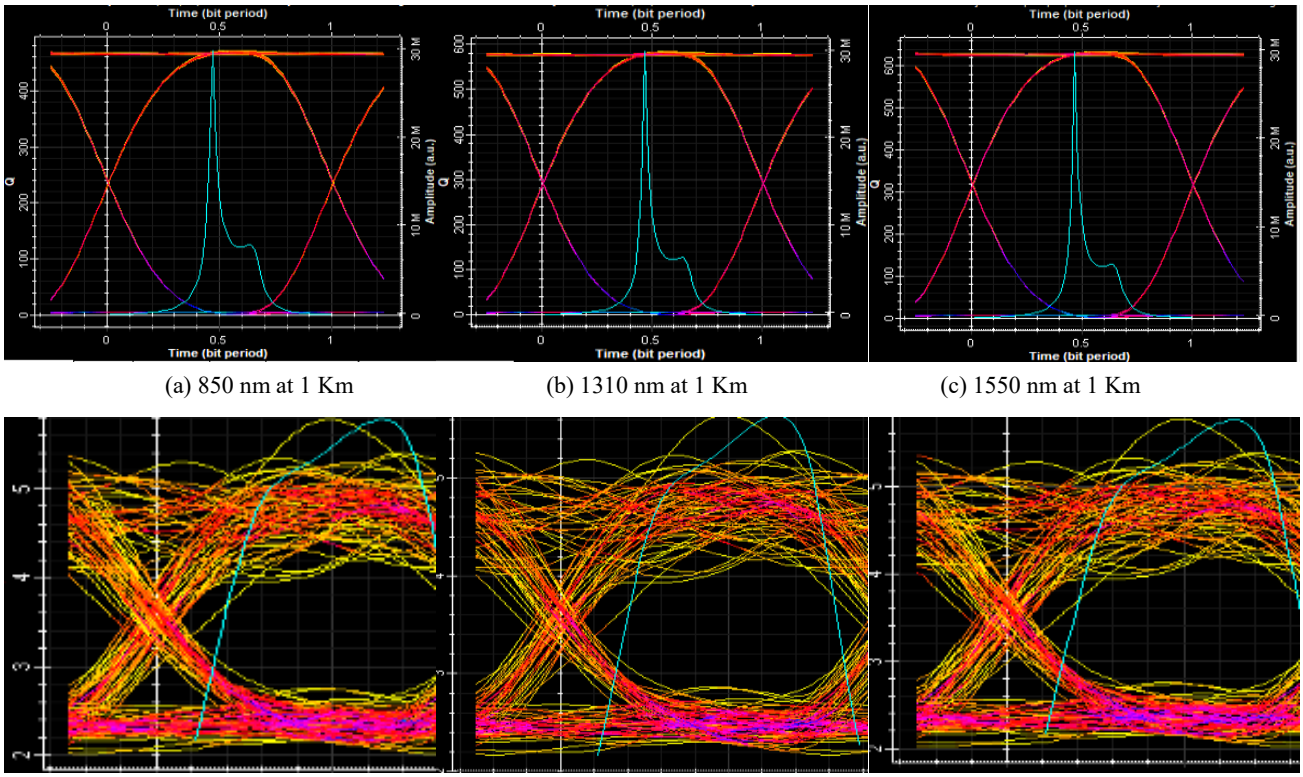

Fig. 18. (a). Eye pattern performance of the SISO-FSO system using a triple boost amplifier at 850 nm, 1310 nm, and 1550 nm under haze conditions (colour online)

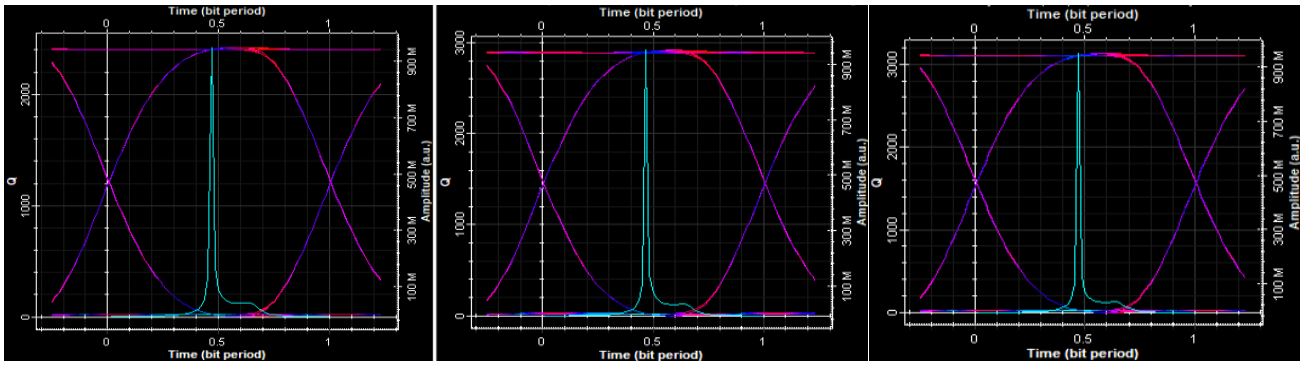

(a) 850 nm at 1 Km (b) 1310 nm at 1 Km (c) 1550 nm at 1 Km

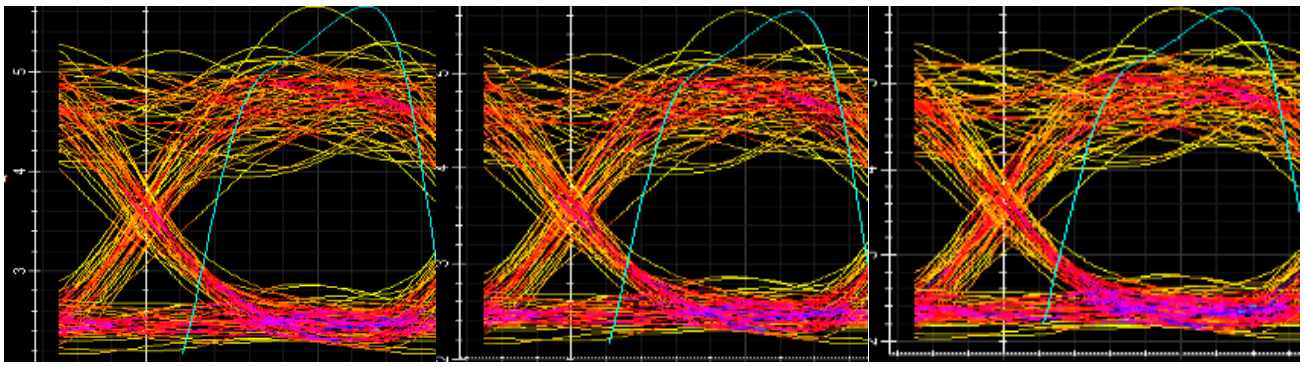

(d) 850 nm at 8.06 Km (e) 1310 nm at 8.25 Km (f) 1550 nm at 8.32 Km

Fig. 18. (b). Eye pattern performance of the 32 × 32 MIMO-FSO system using a triple boost amplifier at 850 nm, 1310 nm, and 1550 nm under haze conditions (colour online)

Figs. 18(a)–(b) depict system performance under haze conditions (specific attenuation = 8.8 dB/km). In this scenario, the SISO-FSO system supports reliable transmission only up to 6.54 km, 6.74 km, and 6.80 km. In contrast, the 32×32 MIMO-FSO system extends the achievable range to approximately 8.06 km, 8.25 km, and 8.32 km with triple-stage amplification.

Overall, the eye-diagram results demonstrate that higher-order MIMO configurations consistently extend the achievable transmission range. That multi-stage optical amplification further improves link reach across all atmospheric conditions considered.

4. Comparative performance analysis across atmospheric conditions

Table 3 consolidates the performance metrics across weather scenarios. Clear conditions offer the best performance, with the 32×32 MIMO configuration utilising triple amplification, achieving a maximum range of 114.8 km. In contrast, rain, fog, and haze limit this range to 14.84 km, 10.48 km, and 8.32 km, respectively. The data demonstrate that:

- Triple-boost amplification consistently outperforms both single and double-boost setups.
- MIMO architectures significantly reduce BER and increase range, particularly under adverse conditions.
- The Q-factor remains stable across all configurations, highlighting the system's robustness.

This analysis confirms the effectiveness of combining spatial diversity with optimised amplification to ensure the reliability of FSO systems under various meteorological conditions.

Table 4 examines the impact of amplifier architecture and operational wavelength on the performance of an FSO-MIMO system under various atmospheric conditions. Across all conditions, longer wavelengths (1550 nm) provide a marginally improved range, especially in clear weather, with an average improvement of 5–9% over 850 nm. Under fog and haze, however, this advantage is diminished by wavelength-dependent scattering.

The triple-boost amplifier configuration offers significant advantages, increasing link distance by up to 33% compared to the double-boost configuration in various MIMO-FSO systems. While MIMO systems enhance FSO performance, their benefits diminish as MIMO levels increase, particularly in adverse environmental conditions such as rain, haze, and fog.

Table 3. Performance evaluation of SISO and MIMO-FSO systems under various weather conditions

Weather Condition	FSO Systems	NRZ-1550 nm_Single Boost Amplifier			NRZ-1550 nm_Double Boost Amplifier			NRZ-1550 nm_Triple Boost Amplifier		
		Range in Km	Q factor	Received power in dBm	Range in Km	Q factor	Received power in dBm	Range in Km	Q factor	Received power in dBm
Clear Weather	SISO	22.20	5.615	-30.970	51.1	5.631	-30.992	86.20	5.645	-30.906
	2×2 MIMO	28.70	5.640	-34.482	57.0	5.625	-34.397	93.0	5.643	-34.487
	4×4 MIMO	30.60	5.619	-37.380	62.8	5.613	-37.789	99.0	5.646	-37.669
	8×8 MIMO	35.10	5.652	-40.622	67.6	5.648	-40.610	104.4	5.620	-40.577
	16×16 MIMO	39.80	5.605	-43.710	73.4	5.631	-43.809	110.6	5.616	-43.737
	32×32 MIMO	43.20	5.647	-48.392	77.2	5.618	-45.988	114.8	5.626	-45.978
Rain	SISO	4.94	5.674	30.907	8.30	5.697	-30.853	11.96	5.694	-30.853
	2×2 MIMO	5.36	5.637	-33.474	8.94	5.651	-34.370	12.66	5.633	-34.497
	4×4 MIMO	6.04	5.659	-37.634	9.54	5.709	-37.692	13.26	5.658	-37.658
	8×8 MIMO	6.52	5.699	40.575	10.06	5.644	-40.614	13.80	5.639	-40.558
	16×16 MIMO	7.06	5.637	-43.677	10.66	5.632	-43.807	14.42	5.631	-43.722
	32×32 MIMO	7.45	5.629	-46.007	11.55	5.604	-48.398	14.84	5.631	-45.972
Fog	SISO	3.70	5.731	-30.848	6.02	5.719	-30.829	8.52	5.712	-30.835
	2×2 MIMO	4.10	5.736	-34.384	6.46	5.659	-34.360	9.0	5.627	-34.504
	4×4 MIMO	4.46	5.735	-37.558	6.88	5.640	-37.762	9.40	5.71	-37.600
	8×8 MIMO	4.80	5.699	-40.575	7.22	5.696	-40.562	9.78	5.600	-40.598
	16×16 MIMO	5.16	5.736	-43.577	7.62	5.760	-43.679	10.18	5.756	-43.595
	32×32 MIMO	5.44	5.627	-46.009	8.17	5.644	-48.092	10.48	5.646	-45.957
Haze	SISO	3.06	5.607	-30.978	4.86	5.737	-30.809	6.80	5.758	-30.787
	2×2 MIMO	3.36	5.765	-34.354	5.20	5.702	-34.317	7.16	5.795	34.332
	4×4 MIMO	3.64	5.785	-37.508	5.52	5.73	-37.648	7.48	5.790	-37.525
	8×8 MIMO	3.90	5.795	-40.462	5.80	5.648	-40.610	7.78	5.621	-40.576
	16×16 MIMO	4.20	5.643	-43.670	6.12	5.618	-43.822	8.10	5.680	-43.672
	32×32 MIMO	4.41	5.625	-46.011	6.32	5.673	-45.930	8.32	5.691	-45.909

Table 4. Performance investigation of MIMO-FSO systems with different amplifier designs and wavelengths

FSO Systems	Amplifier	Range in Km											
		Clear Weather			Rain			Fog			Haze		
		850 nm	1310 nm	1550 nm	850 nm	1310 nm	1550 nm	850 nm	1310 nm	1550 nm	850 nm	1310 nm	1550 nm
SISO	Single	19.10	21.30	22.20	4.54	4.56	4.94	3.42	3.62	3.70	2.82	2.98	3.06
	Double	46.90	49.80	51.10	7.85	8.18	8.30	5.70	5.94	6.02	4.62	4.80	4.86
	Triple	81.40	84.90	86.2	11.48	11.84	11.96	8.20	8.44	8.52	6.54	6.74	6.80
2×2 MIMO	Single	23.40	25.80	28.70	5.10	5.40	5.36	3.68	4.02	4.10	3.14	3.30	3.36
	Double	52.60	55.80	57.00	8.47	8.80	8.94	6.14	6.36	6.46	4.96	5.14	5.20
	Triple	88.20	91.70	93.00	12.14	12.52	12.66	8.66	8.90	9.00	6.90	7.10	7.16
4×4 MIMO	Single	27.10	30.00	30.6	5.62	5.92	6.04	4.18	4.38	4.46	3.42	3.58	3.64
	Double	58.30	61.40	62.80	9.08	9.42	9.54	6.56	6.78	6.88	5.28	5.46	5.52
	Triple	94.30	97.60	99.00	12.78	13.12	13.26	9.06	9.30	9.40	7.22	7.42	7.48
8×8 MIMO	Single	31.40	34.00	35.10	6.08	6.40	6.52	4.50	4.72	4.80	3.68	3.84	3.90
	Double	63.10	66.40	67.60	9.58	9.92	10.06	6.90	7.14	7.22	5.54	5.72	5.80
	Triple	99.50	103.00	104.40	13.32	13.66	13.80	9.44	9.68	9.78	7.52	7.70	7.78
16×16 MIMO	Single	35.90	38.70	39.80	6.62	6.94	7.06	4.86	5.08	5.16	3.96	4.12	4.20
	Double	68.80	72.00	73.40	10.18	10.52	10.66	7.30	7.54	7.62	5.86	6.04	6.12
	Triple	105.70	109.20	110.60	13.94	14.28	14.42	9.84	10.10	10.18	7.84	8.02	8.10
32×32 MIMO	Single	39.20	42.10	43.20	7.00	7.32	7.45	5.13	5.35	5.44	4.17	4.34	4.41
	Double	72.50	75.90	77.20	10.89	10.91	11.50	7.80	7.81	8.17	6.07	6.25	6.32
	Triple	109.8	113.40	114.80	14.34	14.70	14.84	10.14	10.39	10.48	8.06	8.25	8.32

Pointing error poses a significant challenge in FSO communication links, as it directly affects the received optical power and the system's overall reliability. This error typically results from factors such as adverse atmospheric conditions, misalignment between the transmitter and receiver, beam wander induced by turbulence, and structural movements, including building sway. The pointing error at both the transmitter and receiver is estimated to be 1.277 μrad [32].

Table 5. Performance analysis of MIMO-FSO systems with and without pointing error using a triple boost amplifier at 1550 nm

FSO Systems	Range in Km							
	Clear Weather		Rain		Fog		Haze	
	Without Pointing Error	With Pointing Error	Without Pointing Error	With Pointing Error	Without Pointing Error	With Pointing Error	Without Pointing Error	With Pointing Error
SISO	86.20	78.40	11.96	11.16	8.52	7.99	6.80	6.39
2×2 MIMO	93.00	85.10	12.66	11.84	9.00	8.45	7.16	6.75
4×4 MIMO	99.00	91.00	13.26	12.44	9.40	8.86	7.48	7.07
8×8 MIMO	104.40	96.20	13.80	12.99	9.78	9.22	7.78	7.35
16×16 MIMO	110.60	102.40	14.42	13.60	10.18	9.65	8.10	7.67
32×32 MIMO	114.80	106.50	14.84	14.02	10.48	9.91	8.32	7.89

The impact of the link range with and without pointing error is reported in Table 5. In clear weather without pointing error, the link distance extends from 86.2 km for SISO to 114.80 km for 32×32 MIMO. Similar relative improvements are observed under adverse weather conditions, affirming the efficacy of spatial diversity in extending operational range. When a pointing error is introduced, the transmission distance diminishes across all configurations. For instance, under clear conditions, the achievable range decreases from 114.80 km to 106.5 km for the 32×32 MIMO system and from 86.2 km to 78.4 km for SISO. Comparable reductions occur under rain, fog, and haze, highlighting the sensitivity of long-range FSO links to alignment errors. Despite this degradation, higher-order MIMO systems consistently achieve longer transmission distances than SISO systems. The numerical comparison confirms that diversity gain compensates for part of the misalignment loss, while triple-stage amplification helps sustain reliable link operation even in the presence of pointing error.

5. Conclusion

This study presents a comprehensive performance evaluation of FSO communication systems, emphasising the improvements achieved through the integration of MIMO architectures with double- and triple-boost optical amplifier configurations. A detailed comparison between SISO and MIMO systems up to a 32×32 configuration was conducted using three standard optical wavelengths: 850 nm, 1310 nm, and 1550 nm. The results demonstrate that triple-stage amplified MIMO systems consistently outperform their dual-stage counterparts in terms of transmission range and signal quality. Moreover, the spatial diversity provided by MIMO effectively mitigates the adverse effects of atmospheric turbulence and attenuation, resulting in significant enhancements in key performance indicators, such as Q-factor and BER, under various environmental conditions, including clear skies, fog, rain, and haze. Among all tested configurations, the 32×32 MIMO system operating at 1550 nm with triple-stage amplification achieved the longest transmission distance of 114.8 km under clear conditions, while also maintaining strong performance in fog (10.48 km) and haze (8.32 km). These findings highlight the importance of optimising amplifier configurations, transmission wavelengths, and spatial diversity in designing robust and high-capacity FSO communication systems. As a future extension of this work, the integration of adaptive optical amplifier control mechanisms will be explored, enabling dynamic gain adjustment based on real-time atmospheric variations to enhance link reliability and energy efficiency further.

References

[1] A. Malik, P. Singh, International Journal of Optics **6**, 1 (2015).
[2] Arockia Bazil Raj, Arun K. Majumder, IET Communications **13**(16), 2405 (2019).
[3] Isiaka A. Alimi, Paulo P. Monteiro, Sensors **24**(24), 1 (2024).
[4] Pham Tien Dat, Atsushi Kanno, Naokatsu Yamamoto, Tetsuya Kawanishi, Journal of Lightwave Technology **37**(2), 592 (2018).
[5] Celso Henrique de Souza Lopes, Eduardo Saia Lima, Luiz Augusto Melo Pereira, Ramon Maia Borges, Alexandre Carvalho Ferreira, Marcelo Abreu, Journal of Lightwave Technology **39**(2), 406 (2021).
[6] Samir Ahmed Al-Gailani, Mohd Fadzli Mohd Salleh, Ali Ahmed Salem, Redhwan Qasem Shaddad, Usman Ullah Sheikh, Nasir Ahmed Algeelani, Tarik A. Almohamad, IEEE Access **9**, 7353 (2021).
[7] V. Vijayashri, Belgaonkar C. L. Triveni, R. Sundaraguru, Optical and Quantum Electronics **56**(10), 1 (2024).
[8] Arjun Dubey, Davinder Prakash, International Journal of Innovative Technology and Exploring Engineering (IJITEE) **8**(10), 3470 (2019).
[9] Yan Liu, Hongzuo Li, Optical Review **26**, 303 (2019).
[10] Harmeet Kaur, Rajandeep Singh, Ramandeep Kaur, Optoelectron. Adv. Mat. **16**(5-6), 193 (2022).
[11] Mehtab Singh, Journal of Optical Communication **38**(3), 249 (2016).
[12] Ehsan Bayaki, Robert Schober, Ranjan K. Mallik, IEEE Transactions on Communications **57**(11), 3415 (2009).
[13] Hosam Abd Elrazek Mohamed Ali, El-Sayed Soliman A. Said, Mohamed Ebrahim Yousef, International Journal of Optics **3**, 1 (2019).
[14] F. K. Shaker, M. A. A. Ali, F. S. A. Ameer, ECTI Transactions on Electrical Engineering, Electronics, and Communications **17**(2), 130 (2019).
[15] Haroun Errachid Adardour, Samir Kameche, Mehtab Singh, International Journal of Optics **2023**, 1 (2023).
[16] Ali Israr, Adil Israr, Faizullah Khan, Faisal Khan, Wireless Personal Communications **109**(1), 695 (2019).
[17] Shrouk M. Moustafa, Heba A. Fayed, Moustafa H. Aly, Mohamed Mahmoud, Optical and Quantum Electronics **53**, 674 (2021).
[18] E. E. Elsayed, Journal of Optics **54**, 3364 (2025).
[19] Navneet Dayal, Preeti Singh, Pardeep Kaur, Wireless Personal Communications **97**, 6055 (2017).
[20] Deepak Malik, Geeta Kaushik, Amit Wason, Journal of Optics **47**(3), 396 (2018).
[21] Deepak Malik, Geeta Kaushik, Amit Wason, Journal of Optics **47**(2), 235 (2018).
[22] Amit Wason, Deepak Malik, Journal of Optics **49**(3), 298 (2020).
[23] Suresh Kumar, Payal, Pulkit Sharma, Journal of Optics **53**(2), 1264 (2024).
[24] Ebrahim E. Elsayed, Journal of Optics (2024) doi.org/10.1007/s12596-024-02434-4.
[25] R. Palanisamy, K. C. Ramya, J. Roopa Jayasingh, R. Maheswar, P. Roshini, Moustafa H. Aly, Optical and Quantum Electronics **55**, 911 (2023).
[26] E. E. Elsayed, Journal of Optics (2024) doi.org/10.1007/s12596-024-02228-8.
[27] Tagnon P. Okoumassoun, Anita Antwiwaa, Nana K. Gerrar, Journal of Communications **17**(9), 714 (2022).
[28] Ebrahim E. Elsayed, Mohammed R. Hayal, Irfan Nurhidayat, Mohd Asif Shah Abdelrahman Elfikky, Ayman I. Boghdady, Davron Aslonqulovinch Juraev, M. A. Morsy, IET Optoelectronics **18**(1), 1 (2024).
[29] Faizan Shafi, Awanish Kumar, Rangaswamy Nakkeeran, Results in Optics **14**, 100615 (2024).
[30] Ramanababu Challapalli, P. Chitra, Results in Engineering **25**, 103617 (2025).
[31] K. Prabu, D. Sriram Kumar, Optics Communications **343**, 188 (2015).
[32] Jayson K. Jayabarathan, S. Robinson, Journal of Optical Communications **43**(1), 153 (2018).
[33] C. Palaniappan. S. Robinson, MIMO-FSO system for various weather conditions, in "Advances in All-Optical Communication", IOP Publishing Ltd, pp 6.1-6.23, 2024.

*Corresponding author: palani.bharathi31@gmail.com